Cooperative Multimonostatic SAR: A New SAR Configuration for Improved Resolution

Vamsi Krishna Ithapu and Amit Kumar Mishra

***Abstract*—This letter presents a new synthetic aperture radar (SAR) configuration that has been named cooperative multimonostatic SAR (CMM SAR). CMM SAR consists of a battery of monostatic SARs whose flight paths and frequency bands are coordinated in such a way that the final system produces high-resolution images. The point spread function (PSF) of CMM SAR has been used to quantify the gain in resolution as compared to a monostatic SAR system operating under the same k-space area. Three different configurations of CMM SAR have been proposed. Evaluations of these CMM SARs are done, and the results show substantial improvement in performance compared to the conventional monostatic SAR. One of these three CMM SARs is especially the most successful in terms of both gain in performance and simplicity in implementation.**

***Index Terms*—Multiple-input–multiple-output (MIMO) radar, multistatic radar, synthetic aperture radar (SAR) image resolution.**

I. Introduction

SYNTHETIC aperture radar (SAR) systems have been widely used for target detection, tracking, and imaging. They have been designed in various configurations starting from monostatic, bistatic, to the modern multiple-input–multiple-output (MIMO) [1]–[4]. At the heart of a SAR imaging system lies the system impulse response, referred to as point spread functions (PSFs) or impulse response functions (IPRs). As its name suggests, PSF is the SAR imaging-system response for an ideal point target, i.e., the image of a point scatterer. Hence, an ideal PSF for 2-D SAR imaging system, is a 2-D unit impulse function. However, practical radar systems are band-limited, and hence the PSFs are 2-D sinc functions. The more the PSF approaches an ideal unit impulse function, the better the final image quality and resolution. The quality of PSF depends on the bandwidth of the system [5], [6]. The usual procedure of evaluating the performance for an imaging SAR system with a new structure is by first constructing the PSF of the system. Various researchers have developed PSF structures for monostatic and bistatic SAR systems [5], [6].

In the current work, we have tried to investigate the imaging capabilities of a battery of monostatic SAR systems working in a coordinated manner, which we term as cooperative multimonostatic (CMM) SAR system. The coordination among the individual platforms is driven by the drive for a better imaging performance, which is quantified by a better PSF of the system. For a fair comparison with a conventional monostatic SAR system, we try to design the CMM SAR system such that the overall k-space stamp is similar to a reference monostatic SAR system [5]. With this limitation, we propose three different configurations for CMM SAR and compare the performance of each such configuration, for different number of radar platforms, to the conventional monostatic SAR imaging system.

This letter is organized as follows. Section II describes the conventional monostatic SAR system and its PSF. Section III introduces the proposed CMM SAR strategy and constructs its PSF. In the process, three different configurations of CMM SAR are proposed. Section IV evaluates these new CMM SARs and compares their performance to that of conventional monostatic SAR. Section V concludes the letter.

II. Monostatic SAR

Consider a monostatic SAR system with a bandwidth of ΔF and covering an azimuth-angular swath of $\Delta\Phi$. Let the frequency vary from F_1 to F_2 and the azimuth angle vary from ϕ_i to ϕ_f. This defines a patch in the k-space, which determines the resolution of the system. Now, for construction of PSF, we first divide the entire angular swath into P subdivisions. This creation of angle subspaces is for reducing the complexity in achieving a closed-form expression of the PSF (refer to Fig. 1). Let $\Delta\phi_p$'s denote the angular subspace widths and ϕ_p's the central azimuthal angles (with $p = 1, 2, \ldots, P$). Furthermore, let $\Delta\phi_p$'s be such that $\Delta\phi_p = \Delta\phi$ for $p = 1, 2, \ldots, P$. Then, with ϕ_i and ϕ_f, the angular bounds of the k-space, we get $\phi_p = \phi_i + (2p-1)(\Delta\phi/2)$, where $\Delta\phi = (\phi_f - \phi_i)/P$. Using these expressions and constructing the k-space of the monostatic SAR (refer to Fig. 1), we get the PSF as, with $p = 1, 2, \ldots, P$ [5]

$$\mathrm{PSF}_{\mathrm{mono}} = \left(\frac{2\pi}{c}\right)^2 \bar{F}\Delta\phi\Delta F \sum_{p=1}^{P} \mathrm{sinc}\left(\frac{2\pi\Delta F}{c}\psi_{1p}\right) \mathrm{sinc}\left(\frac{2\pi\bar{F}}{c}\Delta\phi\psi_{2p}\right) \quad (1)$$

where

$$\psi_{1p} = x\cos\phi_p + y\sin\phi_p; \psi_{2p} = -x\sin\phi_p + \cos\phi_p. \quad (2)$$

The complete proof of this expression is given in the Appendix. Here, $\bar{F} = (F_1 + F_2)/2$ is the average or nominal frequency of operation, and $\Delta F = F_2 - F_1$ the bandwidth, and c is the speed of light in vacuum. The resolutions Δx and

Manuscript received March 29, 2010; revised May 27, 2010; accepted June 28, 2010. Date of publication July 08, 2010; date of current version August 02, 2010. The work was supported by the Department of Science and Technology (DST), India, through its fast track research program, via sanction number SR/FTP/ETA-34/2007.

The authors are with the Department of Electrical and Computer Engineering, Indian Institute of Technology Guwahati, Guwahati 781039, India (e-mail: v.ithapu@iitg.ernet.in; akmishra@ieee.org).

Digital Object Identifier 10.1109/LAWP.2010.2056670

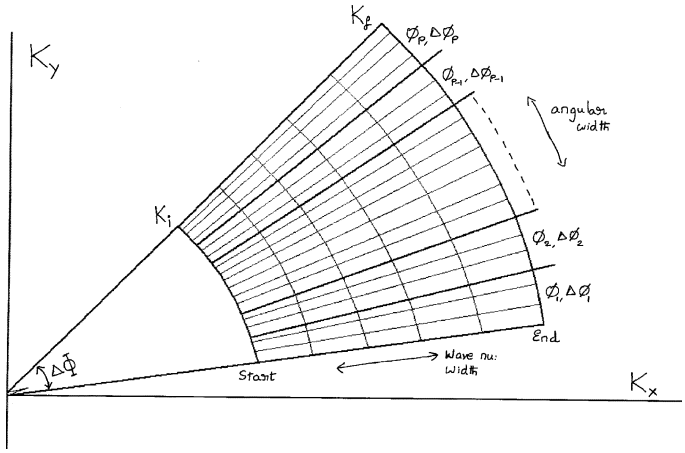

Fig. 1. Monostatic SAR system k-space structure.

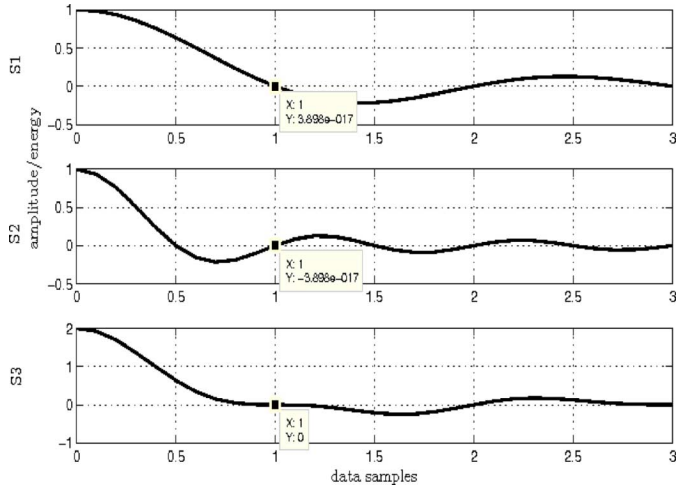

Fig. 2. One-dimensional sinc functions showing null matching strategy. The first null of $S1$ and second null of $S2$ are marked. Observe the main lobe of $S3$ is stronger than that of $S1$ and $S2$, and sidelobe of the same is lower.

Δy of the image, generated with a system with this PSF, are $\Delta x = c/2\Delta F$ and $\Delta y = c/2(P-1)\Delta\phi$. From the equation, we can observe that on the xy image grid, the PSFs of individual cells, from the k-space, align along two normal vectors ψ_{1p} and ψ_{2p} for $p = 1, 2, \ldots, P$. These 2-D sinc functions (P of them) exist along the two vectors of ψ_{1p} and ψ_{2p} and add up to form the final PSF of the system. The first nulls of the final PSF lie on two circles of radii, $r_{1,\mathrm{mono}}$ and $r_{2,\mathrm{mono}}$, given by

$$r_{1,\mathrm{mono}} = \frac{c}{2\pi\Delta F}; \quad r_{2,\mathrm{mono}} = \frac{c}{2\pi\bar{F}\Delta\phi}. \tag{3}$$

Note that their loci are circles as they are independent of the index p. With this background on monostatic SAR and its PSF, we now present our new CMM SAR configuration and derive its PSF.

III. Improving PSF Using CMM SAR Configuration

A. CMM SAR Configuration

Consider a 1-D sinc $S1$ as shown in Fig. 2. Construct another sinc function $S2$, so that the first null of $S1$ coincides with the second null of $S2$. Now, add both of the functions to get $S3$ (Fig. 2). We can observe that for normalized main-lobe amplitudes of 1 for $S1$ and $S2$, the main-lobe amplitude of $S3$ is 2 with peak sidelobes reducing from -0.22 and -0.22 to -0.24, respectively. Hence, an improvement of 6.02 dB in main-lobe resolution is observed with main-to-sidelobe ratio increasing by 6.77 dB. Observe from the figure that the sidelobe amplitudes of $S3$ are lower than that of $S1$ and $S2$. A similar strategy can be applied for 2-D sincs so that the result of adding the respective sinc functions gives rise to enhanced main-lobe amplitude and better main-to-sidelobe ratio.

Hence, adding two sinc functions such that their nulls match improves both main-lobe amplitude and main-lobe-to-sidelobe ratio. This technique is referred to as null matching. Just as two sinc functions are forced to obey this null matching, N different sinc functions divided into $N-1$ overlapping couples can be created such that null matching applies to each couple individually. We call this the generalized null matching (from now on, in this letter, this generalized null matching will be referred to as null matching).

Coming to the SAR imaging case, PSF of the monostatic case is a summation of 2-D sincs, with first nulls aligned in certain formats [refer to (1) and (2)]. The strategy of null matching can be applied here by increasing the number of platforms. This leads to a case where a monostatic transceiver is taken as reference, and from its k-space bounds a configuration with N number of transceivers is created so that the above said null matching applies to all of the N different PSFs so created. From the k-space sense, this means we are given a monostatic system with a given k-space stamp. This is split into N different regions such that the null matching applies to the resulting N different PSFs, hence a new configuration with multiple monostatic transceivers is designed. We refer to this as cooperative multimonostatic (CMM) SAR.

B. PSF for the CMM SAR Configuration

In Section III-A, we have shown that the monostatic PSF, PSF_{mono}, for a given ΔF, $\bar{F}$, $\Delta\phi$, and ϕ_p's is a summation of 2-D sincs with first nulls on the circles of radii $r_{1,\mathrm{tr1,mono}}$ and $r_{2,\mathrm{tr1,mono}}$ (in the subscript $\mathrm{tr1}$ means one platform, as in the conventional monostatic case). For given system parameters, these first null radii are constant. Let us call this PSF $PSF_{\mathrm{tr1,mono}}$. In addition to this, another transceiver platform is operated such that the first null radii of the second one, $r_{1,\mathrm{tr2,mono}}$ and $r_{2,\mathrm{tr2,mono}}$

$$r_{1,\mathrm{tr1,mono}} = 2r_{1,\mathrm{tr2,mono}} \tag{4a}$$

$$r_{2,\mathrm{tr1,mono}} = 2r_{2,\mathrm{tr2,mono}}. \tag{4b}$$

This two-platform case gives improved PSF and hence higher resolution as discussed, and this equation is a null-matching constraint for getting a high-resolution two-transceiver CMM SAR. This same principle can be applied to a system with N platforms created from a monostatic reference system. Now from (3), we see that first nulls are dependent on the frequency and angle bounds of the system, i.e., $\bar{F}$, ΔF and ϕ_p's. As mentioned in Section III-A, the available k-space is divided among the N transceivers here, and hence the Δx and Δy resolutions

of the individual monostatic SAR systems are lower than the original one. However, the aforementioned null-matching condition (extended to N platforms) ensures that the overall PSF has a higher main-lobe amplitude and main-lobe-to-side-lobe ratio. For making N splits in either frequency or angle domain (which then will need N platforms), we have $N+1$ frequency and angle parameters F_n's ($n = 1, 2, \ldots, N+1$), ϕ_n's ($n = 1, 2, \ldots, N$), and ϕ_i (or ϕ_f). To keep the k-space stamp the same as the reference monostatic system, we keep $F_1 = \bar{F} - \Delta F/2$, $F_{N+1} = \bar{F} + \Delta F/2$, $\phi_1 = \phi_i + (\Delta\phi/2)$, and $\phi_{N+1} = \phi_f - (\Delta\phi/2)$. This leaves us with the remaining $2N-2$ unknowns.

We now state the null-matching constraint used to create the final N platform CMM SAR. For $i = 1, 2, \ldots, N-1$

$$r_{1,i,\mathrm{mm}} = 2r_{1,i+1,\mathrm{mm}} \tag{5a}$$
$$r_{2,i,\mathrm{mm}} = 2r_{2,i+1,\mathrm{mm}} \tag{5b}$$

where the first nulls are $r_{1,i,\mathrm{mmst}} = c/2\pi\Delta F_i$; and $r_{2,i,\mathrm{mmst}} = c/2\pi\bar{F}_i\Delta\phi_i$. Using these constraints, we can solve for conditions for the unknown parameters to completely characterize the CMM SAR. Note that P is fixed here, the same as in the reference monostatic case.

Exploring constraints (5a) and (5b) for CMM SAR results in three feasible conditions. The three cases are termed as CMM1, CMM2, and CMM3.

1) Case – 1: CMM1:

$$r_{1,i,\mathrm{mm}} = 2r_{1,i+1,\mathrm{mm}} \tag{6a}$$
$$r_{2,i,\mathrm{mm}} = r_{2,i+1,\mathrm{mm}} \tag{6b}$$
$$\Delta F_{i+1} = 2\Delta F_i \tag{6c}$$
$$\Delta\phi_{i+1} = \Delta\phi_i. \tag{6d}$$

2) Case – 2: CMM2:

$$r_{1,i,\mathrm{mm}} = r_{1,i+1,\mathrm{mm}} \tag{7a}$$
$$r_{2,i,\mathrm{mm}} = 2r_{2,i+1,\mathrm{mm}} \tag{7b}$$
$$\bar{F}_{i+1} = 2\bar{F}_i \tag{7c}$$
$$\Delta\phi_{i+1} = \Delta\phi_i. \tag{7d}$$

3) Case – 3: CMM3:

$$r_{1,i,\mathrm{mm}} = 2r_{1,i+1,\mathrm{mm}};\ r_{2,i,\mathrm{mm}} = 2r_{2,i+1,\mathrm{mm}} \tag{8a}$$
$$r_{2,i,\mathrm{mm}} = 2r_{2,i+1,\mathrm{mm}} \tag{8b}$$
$$\Delta F_{i+1} = 2\Delta F_i \tag{8c}$$
$$\Delta\phi_{i+1} = 2\frac{\bar{F}_i}{\bar{F}_{i+1}}\Delta\phi_i. \tag{8d}$$

In each of the three cases, the unknown values of F_i and ϕ_i can be solved for. It may be noted that the final values of F_i and ϕ_i are different in all the three cases. Hence, we expect the resolution improvement to be different. In CMM1 and CMM2, the frequency space of the reference monostatic system is split into N parts, which can be collected by N monostatic platforms [(6b),(7b)]. Finally, in CMM3 both frequency and angle space are dependently split into N smaller k-space parts [(8b)]. In this case, the overall k-space coverage may be less than that of the reference monostatic case. It can be noted that of the three cases, only CMM3 uses the null constraint [(8a)] completely. It may further be noted that the CMM2 condition may result in making the overall bandwidth of the system higher than that of the reference monostatic case. As mentioned, the three cases may have different improvements in the resolution of the final imaging system. To evaluate this aspect, we construct their PSFs and compare them to the reference monostatic system PSF.

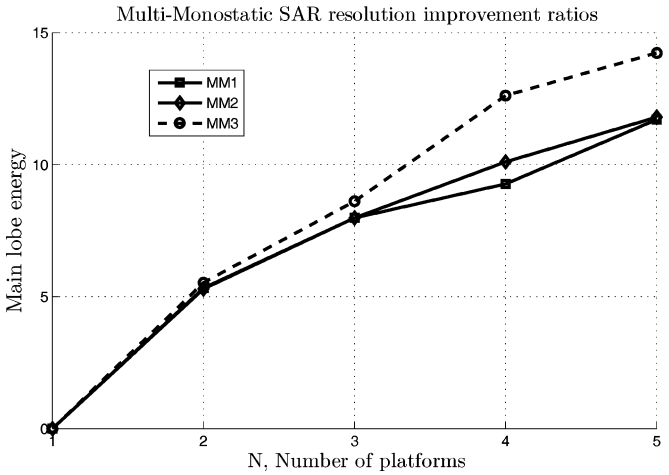

Fig. 3. Main-lobe energy-based comparison of resolution gain for the three CMM SAR configurations. x-axis is the number of platforms, and y-axis shows the main-lobe energy improvement ratio in decibels. Reference monostatic ($N = 1$) is at 0 dB.

IV. Results and Observations

First, we construct a PSF for the reference monostatic system. We consider a monostatic system with central frequency of 3 GHz and bandwidth of 1.2 GHz. The azimuthal angle ranges from $\phi_i = 5^\circ$ to $\phi_f = 30^\circ$. Hence, the imaging grid resolution is approximately a square of 0.12×0.12 m^2. P is taken as 50 so that the angle divisions will be 0.5° each. It can be noted that all our estimates are dependent on P. The PSF of this system is evaluated and taken as the reference. Then, PSFs are constructed for the three types of CMM SARs for different values of N (from $N = 1$ to 5), the number of platforms. $N = 1$ would be a common case for all the three types of CMM SAR, and it is the reference monostatic one. All the measurements done are with respect to this $N = 1$ case.

Figs. 3 and 4 show the PSF characteristics improvement (with respect to the monostatic case) as measured by the main-lobe energies and the main-lobe-to-sidelobe-energy ratios (call it the main-to-side ratio factor), respectively.

As Fig. 3 shows, for all the three cases, the main-lobe energy improvement is almost the same, with CMM3 configuration showing nearly 2 dB more gain for $N = 4$ and $N = 5$. It may be pointed out here that even for simple coherent combination of SAR images from different platforms, the main-lobe energy will increase. However, as depicted in Fig. 4, the main-to-side ratio factors are case-dependent, though all three configurations show substantial improvement as compared to the reference monostatic case. Here, CMM2 performs the poorest, and CMM1 the best till $N = 3$. As N approaches 4 and 5, the ratio factor for CMM2 increases over that of CMM1. An overall gain in resolution is achieved, with ratio factors of the order 25–30 dB for

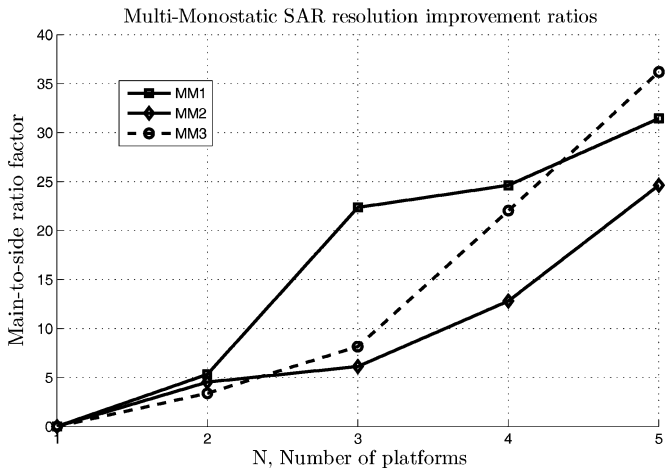

Fig. 4. Main-to-side ratio factor-based comparison of resolution gain for the three CMM SAR configurations. x-axis is the number of platforms, and y-axis shows the main-to-side ratio factor in decibels. Reference monostatic ($N = 1$) is at 0 dB.

$N = 4$. Also, on the average, the case CMM1 performs the best with higher gains in both main-lobe energy and main-to-side ratio factor. This is also the condition that is easiest to implement. This merely requires that multiple monostatic SAR systems be operated for a certain azimuth-angular swath. Individual SAR systems will be needed to operate for lower bandwidth making the individual system complexity lower.

V. Conclusions and Discussions

SAR imaging is a versatile technique used for radar target imaging, and over the past few decades, several configurations of SARs have been proposed and implemented. The current work proposes a cooperative multimonostatic configuration for SAR where the individual SAR systems operate so as to satisfy the generalized null-matching criteria. The resulting configuration gives rise to substantial improvement in resolution of the imaging system as compared to the reference monostatic system. The configuration was termed as CMM SAR, and three feasible modes of operation for this were studied. It was shown that all three CMM SAR configurations give rise to improvement in resolution of the imaging system. It was also shown that CMM1 configuration is the most successful system both in terms of overall gain in performance and in terms of simplicity of the resulting system.

The proposed work has two limitations. First, the proposed scheme has been analyzed at a theoretical level, and certain practical aspects such as motion compensation and data sharing between transmitters/receivers may reduce the improvement shown in this letter. Second, even though the main-to-side factor improves, the resolution achieved using CMM technique will always be lower than the resolution of the individual images.

Our future work aims at testing the proposed CMM SAR configurations on real-time data and also designing its architectural and waveform constraints.

Appendix

PSF (denote it by $\rho(\mathbf{r})$) can be calculated directly from the k-space structure of a SAR system. Consider the k and ϕ bounds to be k_i, k_f, ϕ_i, and ϕ_f. Then, PSF in general is given by [5]

$$\rho(\mathbf{r}) = \int_{k_i}^{k_f} k d\mathbf{k} \int_{\phi_i}^{\phi_f} d\phi e^{2j\mathbf{k}\cdot\mathbf{r}}.$$

We have $\mathbf{r} = x\cos\phi + y\sin\phi$. Call $\Delta\Phi = \phi_f - \phi_i$ as the ϕ-width. Now, for solving the above integral, the ϕ-width should be such that $\Delta\Phi \ll \pi$. However, in general for any SAR imaging system, the angle bounds of k-space do not obey this constraint. Hence, we divide the complete available k-space into P subspaces such that, for each of these subspaces, the ϕ-widths then created satisfy $\Delta\phi_p \ll \pi$ for $p = 1, 2, \ldots, P$. Note here that $\Delta\phi_p$s are the P ϕ-widths of the P subspaces that are created, and their frequency bounds are the same as the total k-space. This division gives us an approximate but closed-form expression of the PSF

$$\rho(x,y) = \int_{\bar{k}-(\Delta k/2)}^{\bar{k}+(\Delta k/2)} k dk \sum_{p=1}^{P} \int_{-\Delta\phi_p/2}^{\Delta\phi_p/2} d\phi e^{2jk(x\cos(\phi_p+\phi)+y\sin(\phi_p+\phi))}$$

where ϕ_p is the central azimuthal angle of the pth subspace. Expanding the arguments in cos and sin, we get two sets of vectors $\psi_{1p} = x\cos\phi_p + y\sin\phi_p$ and $\psi_{2p} = -x\sin\phi_p + \cos\phi_p$. Then, solving this expression, we have the final PSF equation for a monostatic SAR as (note that ψ_{1p} and ψ_{2p} are constant vectors with respect to p)

$$\rho(x,y) = \bar{k}\Delta k \sum_{p=1}^{P} \Delta\phi_p \mathrm{sinc}\left(\Delta k \psi_{1p}\right) \mathrm{sinc}\left(\bar{k}\Delta\phi_p\psi_{2p}\right).$$

References

[1] I. Walterscheid, J. Klare, A. R. Brenner, J. H. G. Edner, and O. Loffeld, "Challanges of a bistatic spaceborne/airborne SAR experiment," in *Proc. EUSAR*, Dresden, Germany, May 2006.

[2] G. Yates, A. M. Horne, A. P. Blake, and R. Middleton, "Bistatic SAR image formation," *IEE Proc. Radar, Sonar Navigat.*, vol. 153, no. 3, pp. 208–213, Jun. 2006.

[3] I. Stojanovic and W. C. Karl, "Imaging of moving targets with multi-staitc SAR using an overcomplete dictionary," *IEEE J. Sel. Topics Signal Process.*, vol. 4, no. 1, pp. 164–176, Feb. 2010.

[4] J. Li, P. Stoica, and X. Zheng, "Signal synthesis and receiver design for MIMO radar imaging," *IEEE Trans. Signal Process.*, vol. 56, no. 8, pt. 2, pp. 3959–3968, Aug. 2008.

[5] R. J. Sullivan, *Radar Foundations for Imaging and Advenced Concepts*. Raleigh, NC: Scitech, 2000, ch. 6.

[6] D. Massonnet and J. C. Souyris, *Imaging With Synthetic Aperture Radar*. Lausanne, Switzerland: EPFL Press, 2008, ch. 2.